https://doi.org/10.48048/tis.2023.5839

Growth and Exploration of Inorganic Semiconductor Electron and Hole Transport Layers for Low-Cost Perovskite Solar Cells

Shukri Rashed[1,2], Vishnu Vilas Kutwade[1], Ketan Prakash Gattu[3], Ghamdan Mahmood Mohammed Saleh Gubari[1] and Ramphal Sharma[1,3,4,*]

[1]*Department of Physics, Dr. Babasaheb Ambedkar Marathwada University, Maharashtra, India*
[2]*Department of Physics, University of Aden, Aden, Yemen*
[3]*Department of Nanotechnology, Dr. Babasaheb Ambedkar Marathwada University, Maharashtra, India*
[4]*Department of Physics, IIS (Deemed to be University), Rajasthan, India*

([*]Corresponding author e-mail: rps.phy@gmail.com)

Received: 1 September 2022, Revised: 9 October 2022, Accepted: 16 October 2022, Published: 19 June 2023

Abstract

The perovskite exhibited outstanding performance and was a promising alternative material for a low-cost, high power conversion efficiency (PCE) solar cell application. To avoid the high-cost organic materials as electron transport layers (ETL) and hole transport layers (HTL) in perovskite solar cells (PSCs), here introduce the inorganic semiconductor nanomaterials ZnS and CuS work as an ETL and HTL, respectively. In this work, we selected chalcogenides such as zinc sulfide (ZnS) and copper sulfide (CuS) as the 2-electron and hole transport layers and utilized them for perovskite solar cell application. For the proposed cell structure FTO/ZnS/perovskite ($CH_3NH_3PbI_3$)/CuS/Ag, the deposition of layers has been achieved via different techniques such as thermal evaporation, spin coating and doctor blade, respectively. X-ray diffraction and Field effect scanning electron microscopy (FESEM) with Energy-dispersive X-ray spectroscopy were used to characterize the structural and morphological properties of the prepared samples. UV-Visible spectrophotometer and current density-voltage curve were used to measure the optical and electrical parameters of the deposited layers, respectively. From the J-V characteristics, for the proposed and fabricated PSCs, the estimated PCE is about 0.28 %, open-circuit voltage (V_{OC}) = 0.29 V, and short-circuit current density (J_{SC}) = 3.96 mA/cm^2. The results are good and the inorganic nanomaterial layers used in this study are promising for future studies.

Keywords: Spin-coating, Vacuum thermal evaporation, Perovskite, Thin film solar cell, Semiconductor, Nanomaterials, I-V

Introduction

Solar cells are considered the cleanest way to produce electricity from the natural source which is the sun. As this device does not cause any emission of polluting gases to the environment. Currently, crystalline silicon-based photovoltaic cells dominate the commercial market despite their high costs. The issue of solar cells has grown in popularity a source of interest for researchers in the advancement of photovoltaic cells with the lowest cost, high stability and high efficiency. For this purpose, and since the initial presentation of solar cells containing metal halide perovskite [1], researchers have been interested in this type of PSCs. These cells showed outstanding performance and a promising alternative and low-cost photovoltaic cells [2,3], with additional layers of charge transfer as catalysts which is important in improving their efficiency [4], and resulted in certified PCE of more than 23 % [5]. In particular, the search for charge transfer materials for electrons and holes has become critical in enhancing the performance of perovskite solar cells. For example, common hole transfer materials (HTMs) are generally limited to octakis (4-methoxyphenyl)-9,9′-spirospirobi [9H-fluorine]-2,2′,7,7′- tetramine (spiro-OMeTAD) [6], polymers [7,8], and a limited number of conjugated molecules [9-11]. Whereby it showed limited stability and a high cost of materials [12-14]. Because of its low mobility, organic HTM usually requires the incorporation of additional activated materials, cobalt or lithium salts, to develop the properties of the responsible carrier, however it degrades the photoactive material [15]. To attain high levels of commercialization for perovskite cells in the future the search for stable, efficient and lower-cost HTM has become vitally important. In this context, inorganic HTM represents a good alternative due to its high conductivity, hole mobility, low cost, and its thermal and

chemical stability such as Cu_2O [16], NiO [17], and CuSCN [18], which properly require processing at high temperatures. However, at lower temperatures, it is applied with Spiro-OMeTAD [19,20]. Thus, a limited number of reports used inorganic materials such as HTM. In addition, treatment is carried out in polar solvents for these materials, which leads to the destruction of the perovskite layer easily. This leads to a limitation of its application due to the formation of the n-i-p device. In this respect, Sulfide derivatives are an interesting class because of their optical and electronic properties, conductivity, high p-type charge transferability and chemical stability [21,22], CuS has been effectively used in various optoelectronic applications due to its electrical characteristics, including adjusting the work function of ITO [23], and passivating the HTM/metal interface by CuS sublimation [19]. Furthermore, CuS acts as an inorganic moisture barrier [19], potentially preventing perovskite compounds from deteriorating. Despite these advantages, CuS has yet to be employed as the only inorganic HTM, owing to a paucity of perovskite-compatible elemental solutions [24]. On the other hand, to obtain better, low cost and more stable performance in the work of perovskite solar cells, the researchers are interested in studying the nature of the electron transfer materials, which act as an electron transfer layer (ETL) in perovskite, such as TiO_2, ZnO and PCBM [25].

Although TiO_2 has achieved good results and is the most commonly used and research is continuing to develop and enhance this area to achieve better performance in improving a PCE-enhancement pathway for perovskite solar cells [26,27]. In this context, ZnS is a chalcogen semiconductor belonging to the II-VI family of semiconductors [28], and has received increasing interest because of its numerous uses in electroluminescent devices [29], ultraviolet emitting diodes [30], and cathode layers and insulating layers in solar. It has a wide-bandgap range of 3.5 - 3.8 V at room temperature [31,32]. On the other hand, zinc-based materials were studied as the electron transfer layer for low-temperature devices, in PSCs devices and became a possible material for a variety of applications because of their high transparency and high mobility of electrons. Therefore, ZnS and CuS were introduced into the PSCs [33,35]. The purpose of this research work is to present the obtained PSCs results using thin layers of inorganic materials ZnS and CuS. Where ZnS work as ETL and CuS works as HTL in PSCs. The individual semiconductor layers were fabricated via a simple chemical bath deposition technique at low temperatures. Structural, optical, morphological and electrical studies of the prepared sample are carried out via X-ray diffraction (XRD), UV-Visible spectroscopy, Field-Effect Scanning Electron Microscope (FESEM) and Energy Dispersive X-ray Analysis (EDAX) and I-V characteristics, respectively.

Materials and methods

Zinc sulfide powder (CAS NO.1314-98-3) from Reg-LABOGENS(India), Fluorine-doped tin oxide (FTO), size 50×50×1.1 mm^3 from Shilpa Enterprises-India, Lead Iodide (99.99 %) trace metals basis (CAS 10101-63-0), Methylamine Hydroiodide (Low water content) (CAS 14965-49-2.) TCI-Japan, Triethanolamine 99 % LOBA CHEMIE-India, Cupric sulfate M.W 159.12 gm/mol from Fisher scientific-India, ammonia solution (NH_3 25 %) from Molychem-India, N-methyl-2-pyrrolidone, poly (vinylidene fluoride) from Alfa Aesar-USA and N, N-dimethylformamide (DMF) from SDFCL -India were purchased. One of the most important aspects in the deposition of the homogeneous and uniform thin film is the cleaning of the substrate to get better adhesion and promising results. In this report, Fluorine-doped tin oxide (FTO) substrates are cleaned and washed with deionized water. After that, FTO substrates were immersed in acetone for 10 min, then washed with deionized water several times, then, the substrates were placed inside an ultrasonic bath for 15 min, and finally dried at room temperature.

ZnS layer has been deposited by vacuum thermal evaporation at the JEOL JEE-4C vacuum evaporator with the function of electron transport layer for perovskite solar cell. At the temperature of the FTO glass substrate T_{sub} = 300 K, the evaporation mass was about 20 mg of ZnS powders and the Vacuum pressure was approximately 72×10^{-4} torr. The electric current through the evaporator was about 50 A with a time deposition of 20 min. After the deposition process was completed, the device was gradually turned off for some time, taking into consideration the conditions of thermal equilibrium and pressure inside the device. The sample was good and homogeneous as well.

To prepare perovskite $CH_3NH_3PbI_3$ 462 mg of PbI_2 were mixed with 158 mg CH_3NH_3I and then dissolved in 1 mL DMF. The solution was stirred at 70 °C for 1 h to obtain a well-mixed solution. To prepare copper sulfide CuS nanoparticles (NPs), we used chemical bath deposition by using (0.01 M) cupric sulfate ($CuSO_4$) dissolving in 25 mL distilled water stirred for 30 min, (0.03 M) thiourea dissolving in 25 mL distilled water that stirred for few minutes. Drops of ammonia (4 mL) were added to the solution of copper sulfide drop by drop to get a clear and homogeneous solution, after that triethylamine($N_{15}H_6C$) was added to the solution as a complex agent. The solution that was produced by mixing thiourea with the

copper sulfate was placed in a bath at a temperature (of 40 - 50 ℃) for 45 min. After the reaction is completed, the solution is filtered by using filter paper to get the desired powder, which is dried at room temperature. Then, calcined in an oven at 150 ℃ for 2 h and finally, the CuS powder is crushed and used for further characterization.

The 1×1 cm^2 of the FTO/ZnS thin film was prepared by vacuum thermal evaporation and placed on a spin-coating machine, then 30 drops of $CH_3NH_3PbI_3$ solution were added and spin-coated on a 1 cm^2 FTO/ZnS substrate under 2,000 rpm for 45 s. The films were heated by a hot plate at 100 ℃ for 20 min. The color of the film changed from yellow into dark brown by heating, after that it cooled at room temperature. For the deposited CuS layer on the perovskite layer by doctor blade method, we take (0.28 gm (95 %wt.) of the prepared powder of CuS NPs by CBD method), which was dissolved in (5 %wt poly (vinylidene fluoride) with few drops of N-Methyl-2-pyrrolidone (NMP) then stirred for 6 h to obtain a good and homogeneous solution, after that a small amount of this solution i.e., CuS layer is deposited on the perovskite layer by using doctor blade quickly. The samples were annealed in the oven at 100 °C for 1 h, after that it cools to room temperature. These samples are kept in a tight box and it is ready to study their characterization, the detailed method is presented in **Figures 1** and **2** shows the diagram of the proposed perovskite cell structure, band edge diagram and perovskite thin films after and before annealing [37].

The thickness of thin films was used most common method for measuring the thickness of the film and measuring the mass of the substrate before deposition and after, and calculating the mass difference, as well as in terms of the density of the material and the area of the film, through the following equation;

$$t = \frac{\Delta m}{\rho * A}, \quad \Delta m = m_1 - m_2 \tag{1}$$

where Δm is a mass difference of the substrate, m_1 mass of substrate before deposition, and m_2 mass after deposition. t is film thickness A is the respective area of the deposited film and ρ is the bulk density of the deposited material.

Here ρ is 4.09 gm/cm^3 for ZnS, ρ is 4.2864 gm/cm^3 for $CH_3NH_3PbI_3$, and ρ is 4.76 gm/cm^3 for CuS. Therefore the thicknesses of the films were approximated 50, 200 and 150 nm for ZnS, $CH_3NH_3PbI_3$ and CuS, respectively.

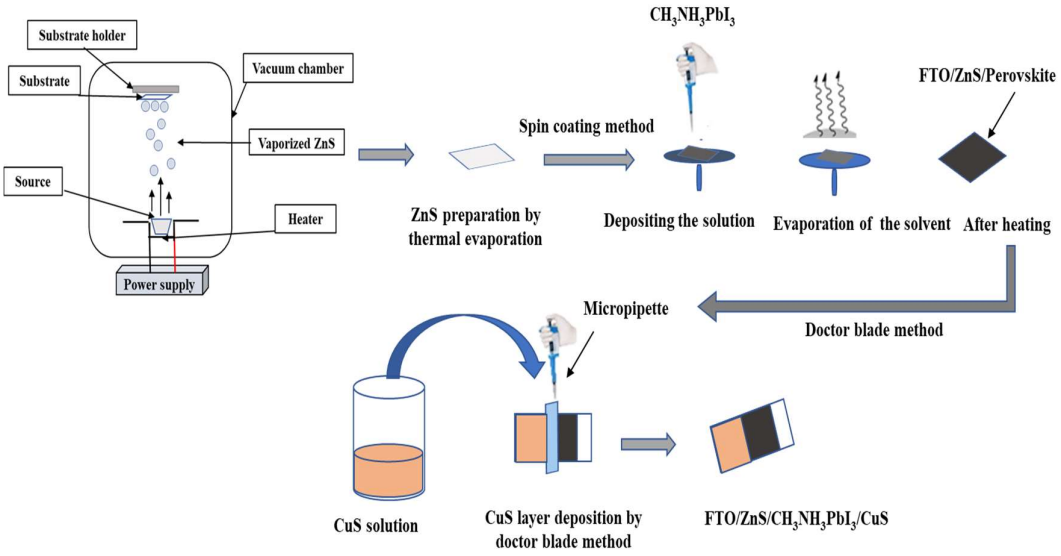

Figure 1 Pictorial diagram of the perovskite device fabrication.

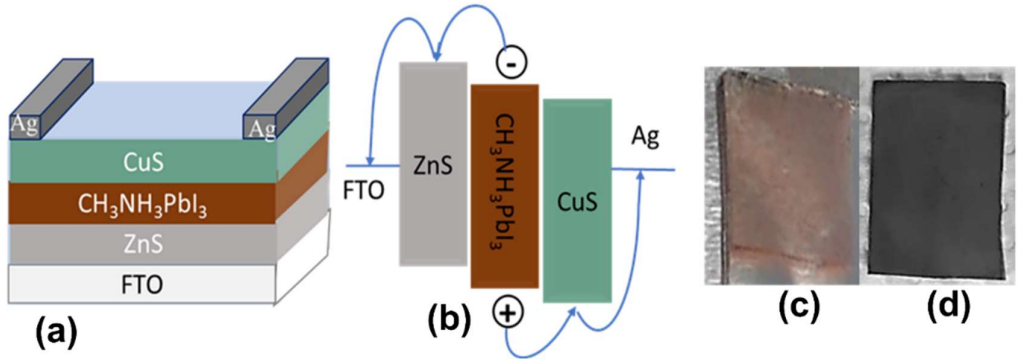

Figure 2 (a) device structure FTO/ ZnS/$CH_3NH_3PbI_3$/CuS/Ag solar cells, (b) band-edge diagram of the proposed cell structure, (c) and (d) images of perovskite films before & after annealing.

Results and discussion

The method of transforming solar energy into electrical energy occurs in phases at the cell level. When the photons with energies greater than the width of the bandgap are absorbed and produce excited electrons, which are then separated from the perovskite layer, after which the excitons diffuse to the regions where charge dissociation or separation of electrons and holes occurs, and the resulting charges are transported to the electrodes [37].

X-ray diffraction patterns

X-ray diffraction is a distinctive feature of the material that contributes to determining the structure, shape, size and direction of the unit cell, as well as detecting crystal defects. **Figure 3** depicts the XRD pattern of the (FTO/ZnS/Perovskite/CuS) layers. **Figure 3(a)** (black) represents the X-ray pattern of the CuS thin film deposited by doctor baled method on the FTO substrate and shows the significant peaks at 29.5, 56.01 and 66.04 ° which correspond to (102), (001) and (206), respectively and show hexagonal phase that excellently agreed with (JCPDS File No. 850-620). The XRD patterns of FTO/ZnS thin films are shown in **Figure 3(b)** (blue). The X-ray diffraction pattern for the ZnS layer shows a hexagonal phase and the diffraction peaks at 28.6, 47.52, 56.46, 66.46 and 76.17 ° which corresponds to (008), (110), (118), (101) and (212), respectively and perfectly matched with (PDF# 720-63).

The XRD pattern of FTO/ZnS/Perovskite/CuS thin film is shown in **Figure 3(c)** (red) fabricated by spin-coating for 1:1 M from PbI_2:MAI, the XRD pattern for the $CH_3NH_3PbI_3$ shows the strong and main diffraction peaks at 20.02, 24.50, 31.80, 34.93, 40.54, 43.08, 50.16 and 60.58 ° which correspond to (200), (202), (141), (240), (224), (060), (440) and (404) reflections and they indicate the presence of $CH_3NH_3PbI_3$ NPs that agreed with (JCPDS# 07-0235 and 10-0737) [38-41]. The detailed calculations of lattice parameters of FTO/ZnS/Perovskite/CuS thin film are shown in **Table 1**.

Table 1 Lattice parameters of FTO/ZnS/Perovskite/CuS thin film.

Sr. No.	2θ (degree)	B (degree)	D (nm)	d (Å)	Miller indices (hkl)
			Perovskite		
1	20.02	0.12631	66.76530	4.434989	(200)
2	24.50	0.14236	59.68911	3.633229	(202)
3	31.80	0.18471	46.74661	2.813886	(141)
4	34.93	0.17827	48.83057	2.568579	(240)
5	40.54	0.21328	41.50396	2.225147	(224)
6	43.08	0.21502	41.51317	2.099656	(060)
7	50.16	0.22528	40.69675	1.818637	(440)
8	60.58	0.25732	37.37233	1.528401	(404)

Sr. No.	2θ (degree)	B (degree)	D (nm)	d (Å)	Miller indices (hkl)
	Average (D)		**47.88973**		
			ZnS		
9	28.60	0.22947	37.32846	3.121025	(008)
10	47.52	0.35348	25.64083	1.913323	(110)
11	56.47	0.44255	21.29783	1.629482	(118)
12	65.90	0.1002	98.53035	1.417320	(101)
13	67.17	0.1899	52.48902	1.393577	(212)
	Average (D)		**47.05730**		
			CuS		
14	29.50	0.22528	38.10856	3.027824	(102)
15	56.01	0.44255	21.25180	1.641768	(001)
16	66.04	0.07515	131.8955	1.414654	(206)
	Average (D)		**63.75194**		

The widths of the matching X-ray pattern peaks were used to calculate the crystallite size. X-ray diffraction analysis was used to investigate the phase composition and structure of the film. The X-ray diffraction pattern of the FTO slice is shown in the all figures with a black dashed line and displayed the highest reflection peak were 26.5, 33.6, 37.7 51.7 and 61.9 ° which corresponds to (110), (101), (200), (211) and (310) which matched with (JCPDS# 00-046-1088) [42,43].

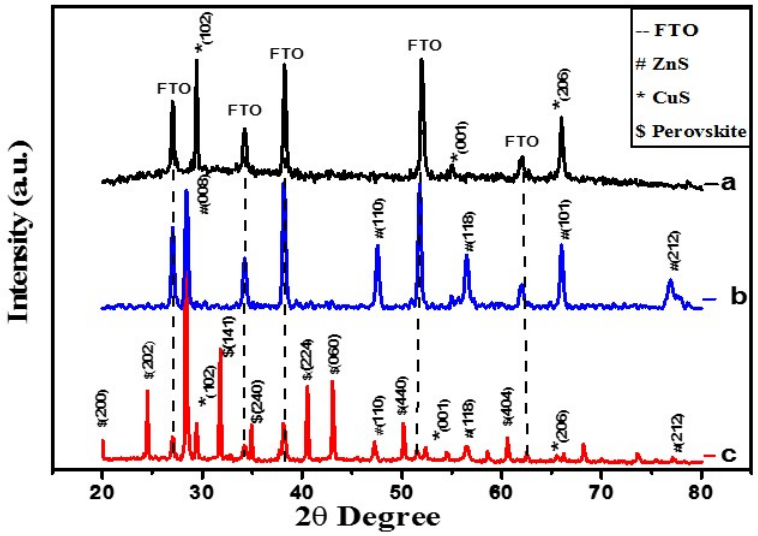

Figure 3 XRD pattern of a) FTO/Cus, b) FTO/ZnS and c) FTO/ZnS/perovskite/CuS.

Morphological and elementary details

Field-Effect Scanning Electron Microscope (FESEM) and Energy Dispersive X-ray Analysis (EDAX) were utilized for the morphological images and the percentage of the constituents of the deposited layers as depicted in **Figure 4**. From **Figure 4(a)** we notice that the zinc sulphide (ZnS) NPs are regular and homogeneous aligned along the surface area of the substrate. Where the particles appeared spherically agglutinated with rose-like crystallization and the particle size is somewhat similar in diameter. The results of the elementary percentage examination in EDAX spectra confirmed the existence of the Zinc and Sulfur

elements indicating the formation of the zinc sulphide NPs layer [44], as shown in Figure 4a. Similarly, it is obvious from **Figure 4(b)**, the surface morphology of the $CH_3NH_3PbI_3$ layer that was deposited by the spin coating approach appears entangled with each other as a well-adjusted and symmetrical fibrous network. This fibrous crosslinking enhances the presence of lead iodide particles which is in good agreement with the previous study [45]. On the other hand, in the results of the EDAX analysis, the elements appeared in the form of the perovskite material $CH_3NH_3PbI_3$ constituents, which verified the presence of that substance in the device composition which is represented in **Figure 4(b)**. Finally, the CuS morphology with aggregated sphere-like structure tends to be self-assembled generating hexagonal nano-plates, as seen in the FESEM image (**Figure 4(c)**). However, the end-to-end growth and development of hexagonal nano-plates with inherently anisotropic CuS structure were hindered by the low reaction temperature and short reaction time [46]. The spectra of EDAX displayed the presence of Copper and Sulfur elements as the components of CuS as shown in **Figure 4(c)**. The EDAX spectra and the Table of the percentage of all elements of the ZnS/$CH_3NH_3PbI_3$/CuS device are presented in **Figure 4(d)** and confirmed the existence of components indicating the successful fabrication.

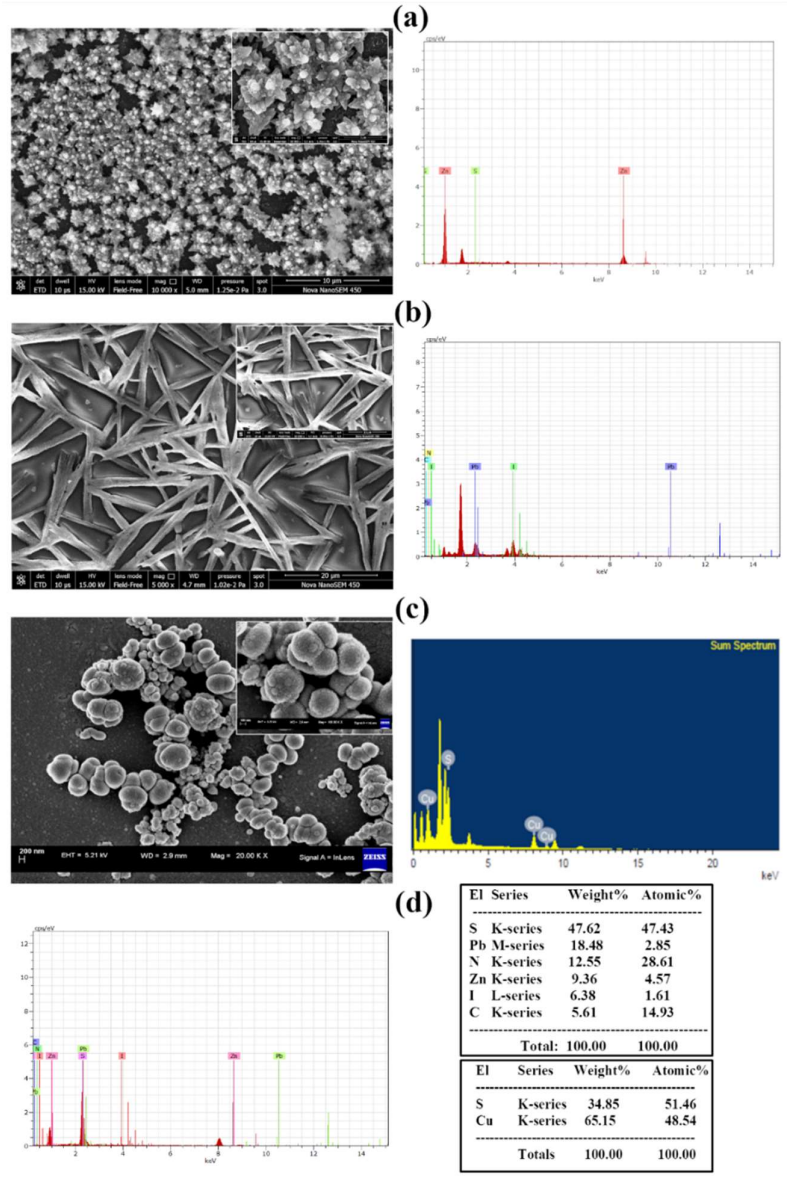

Figure 4 FESEM images with EDAX spectra for (a) ZnS Layer, (b) Perovskite ($CH_3NH_3PbI_3$) Layer, (c) CuS Layer and (d) EDAX spectra of all elements of the ZnS/$CH_3NH_3PbI_3$/CuS device.

Optical studies

The optical density and bandgap energy of fabricated perovskite solar cell devices are shown in **Figure 5**. The absorption spectra and bandgap energy of ZnS thin-film embedded with the estimated energy band gaps plot are represented in **Figure 5(a)**. The absorption spectra showed a substantial increase in the visible light at 335 corresponding to the bandgap values are 3.72 eV as calculated using Tauc's equation [47];

$$\alpha = \frac{\alpha_0(h\nu - E_g)^n}{h\nu} \quad (2)$$

where α_0 is the absorption coefficient, h is Plank's constant (h = 6.626×10^{-34} m^2 kg/s), ν is the frequency of the incident light and E_g is the bandgap energy and n is the exponent which has the value of 1/2 and 2 for the direct and indirect transition, respectively. The $CH_3NH_2PbI_3$ Perovskite absorption spectrum displayed a remarkable absorption in the visible light region onset in wavelength around ~760 nm, with redshift and the calculated bandgap energy found to be 1.6 eV as shown in **Figure 5(b)** and matched with results reported elsewhere [48].

The optical study of the prepared CuS using the doctor blade route is also carried out using a photo-spectrophotometer and the characteristic absorbance wavelength launched at around ~570 nm which directly matched with 2.2 eV bandgap energy value as shown in **Figure 5(c)** and excellently agreed with the results reported by [46]. Moreover, the $CH_3NH_2PbI_3$ Perovskite has a noticeable absorption peak and a significantly reduced bandgap, making it an efficient device for absorbing visible light and effectively substituting its rich carrier charges to the ZnS and CuS layers when they are exposed to visible light [49].

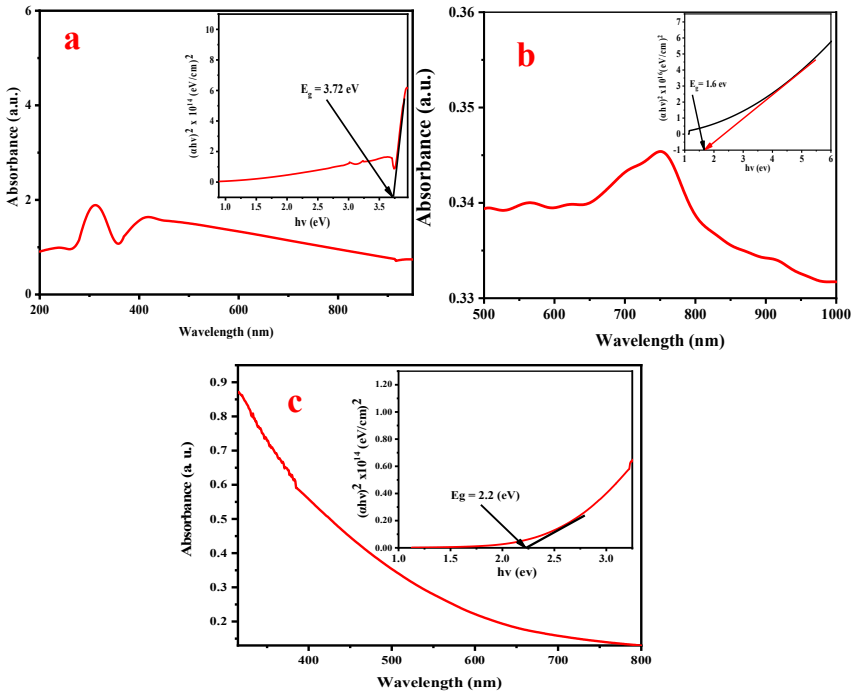

Figure 5 Optical absorption spectrum with inset of bandgap energy of (a) ZnS, (b) perovskite and (c) CuS.

I-V characteristics

The electrical properties of the fabricated device "FTO/ZnS/Perovskite ($CH_3NH_3PbI_3$)/CuS /Ag" were studied from the current density-voltage (J-V) curves using the Keithley 2400 I-V source meter interfaced with Class AAA Solar Simulator under dark and under light illumination conditions.

The power conversion efficiency (η) of the solar cells can be calculated using the following equation [47,50];

$$\eta = \frac{J_{sc}\times V_{oc}\times FF}{P_{in}} \times 100 \quad (3)$$

where (*J*sc) is short-circuited current, (*V*oc) open-circuit voltage, (FF) fill factor, and P_{in} is the power density of incident light. It is obvious from **Figure 6** that after exposing the device to the light through the optical window, the light-activated the perovskite layer and interact with the photons and the charge carriers i.e., electrons and holes biased, where the electrons transported toward ZnS and the holes transported toward CuS. From this principle of working, we got the power conversion efficiency (PCE) which equals 0.28 % and all the calculated parameters are presented in **Table 2**. The acquired efficiency is very small due to the nature of perovskite which is affected by humidity, contamination in growth and environmental factors causing the reduction in its efficiency. This will be improved by post-deposition annealing in the different ambiances, but solar cells present here more stability concerning characterizations.

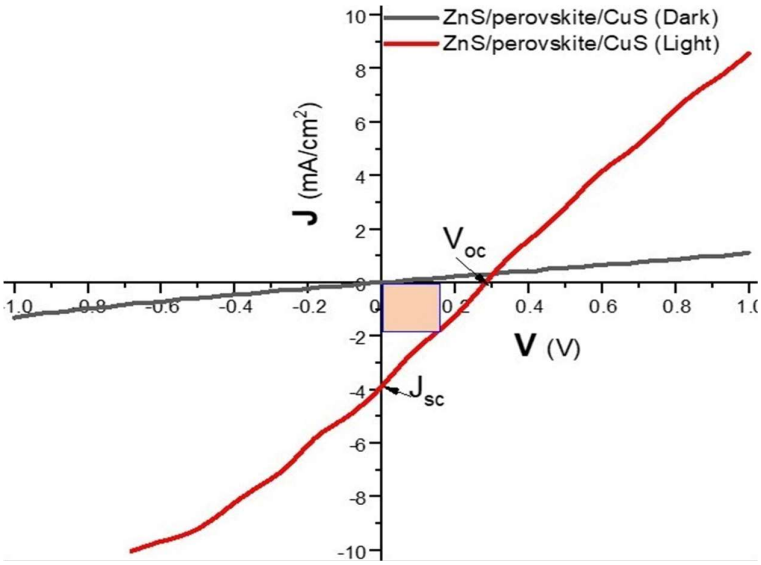

Figure 6 Current density-voltage curve of FTO/ZnS/Perovskite ($CH_3NH_3PbI_3$)/CuS/Ag device.

Table 2 The calculated solar cell parameters for the fabricated FTO/ZnS/Perovskite/CuS/Ag device under exposure to illumination.

Perovskite material	Device structure	V_{oc} (v)	J_{sc}(mA/cm^2)	FF	Power input (MW/cm^2)	PCE (%)
$CH_3NH_3PbI_3$	FTO/ZnS/$CH_3NH_3PbI_3$/CuS	0.29	3.96	0.25	100	0.28

Conclusions

The FTO/ZnS/Perovskite/CuS/Ag device has been successfully fabricated through thermal evaporation, spin coating and doctor blade processes, respectively. The temperature of annealing is 100 °C. The morphology and composition of the films are characterized via FESEM, XRD and I-V to confirm the characteristic features. The structural and morphological characterization displayed ZnS particles in spherically agglutinated with rose-like crystallization and the particle size is slightly analogous in diameter. While the perovskite ($CH_3NH_3PbI_3$) layer appeared symmetrical fibrous network and entangled as a well-adjusted. The CuS morphology with aggregated sphere-like structure tends to be self-assembled generating hexagonal nano-plates. The measured band gap displayed 3.72, 1.6 and 2.2 eV for ZnS, perovskite and CuS, respectively. The calculated power conversion efficiency (PCE) is around 0.28 %, the resulting value was low but the used materials in this study are promising and developable in futuristic studies.

Acknowledgments

Authors are thankful to the Department of Physics, Dr. Babasaheb Ambedkar Marathwada University Aurangabad for providing laboratory facilities. Authors are also thankful to the Inter University Accelerator Centre (IUAC), New Delhi, India and UGC-DAE CSR, Indore for the characterization facilities.

References

[1] A Kojima, K Teshima, Y Shirai and T Miyasaka. Organometal halide perovskites as visible-light sensitizers for photovoltaic cells. *J. Am. Chem. Soc*. 2009; **131**, 6050-1

[2] H Snaith and J Perovskites. The emergence of a new era for low-cost, high-efficiency solar cells. *J. Phys. Chem. Lett*. 2013; **4**, 3623-30

[3] JP Correa-Baena, A Abate, M Saliba, W Tress, TJ Jacobsson, M Grätzel and A Hagfeldt. The rapid evolution of highly efficient perovskite solar cells. *Energ. Environ. Sci.* 2017; **10**, 710-27

[4] W Chen, Y Wu, Y Yue, J Liu, W Zhang, X Yang, H Chen, E Bi, I Ashraful, M Grätzel and L Han. Efficient and stable large-area perovskite solar cells with inorganic charge extraction layers. *Science* 2015; **350**, 944-8

[5] WS Yang, BW Park, EH Jung, NJ Jeon, YC Kim, DU Lee, SS Shin, J Seo, EK Kim, JH Noh and SI Seok. Iodide management in formamidinium-lead-halide-based perovskite layers for efficient solar cells. *Science* 2017; **356**, 1376-9

[6] AT Murray, JM Frost, CH Hendon, CD Molloy, DR Carbery and A Walsh. Modular design of SPIRO-OMeTAD analogues as hole transport materials in solar cells. *Chem. Comm.* 2015; **51**, 8935-8

[7] JC Brauer, YH Lee, MK Nazeeruddin and N Banerji. Charge transfer dynamics from organometal halide perovskite to polymeric hole transport materials in hybrid solar cells. *J. Phys. Chem. Lett.* 2015; **6**, 3675-81

[8] GW Kim, J Kim, GY Lee, G Kang, J Lee and T Park. A strategy to design a donor-π-acceptor polymeric hole conductor for an efficient perovskite solar cell. *Adv. Energ. Mater.* 2015; **5**, 1500471.

[9] LB Chang, CC Tseng, JH Lee, GM Wu, MJ Jeng, WS Feng, DW Chen, LC Chen, KL Lee, E Popko, L Jacak and K Gwozdz. Preparation and characterization of $MoSe_2/CH_3NH_3PbI_3$/PMMA perovskite solar cells using polyethylene glycol solution. *Vacuum* 2020; **178**, 109441.

[10] C Giansante, R Mastria, G Lerario, L Moretti, I Kriegel, F Scotognella, G Lanzani, S Carallo, M Esposito, M Biasiucci, A Rizzo and G Gigli. Molecular-level switching of polymer/nanocrystal non-covalent interactions and application in hybrid solar cells. *Adv. Funct. Mater.* 2015; **25**, 111-9.

[11] NS Kumar and KC Naidu. A review on perovskite solar cells (PSCs), materials and applications. *J. Mater.* 2021; **7**, 940-56.

[12] Y Wang, Z Xia, J Liang, X Wang, Y Liu, C Liu, S Zhang and H Zhou. Towards printed perovskite solar cells with cuprous oxide hole transporting layers: A theoretical design. *Semicond. Sci. Tech.* 2015; **30**, 054004.

[13] CY Chang, YC Chang, WK Huang, WC Liao, H Wang, C Yeh, BC Tsai, YC Huang and CS Tsao. Achieving high efficiency and improved stability in large-area ITO-free perovskite solar cells with thiol-functionalized self-assembled monolayers. *J. Mater. Chem. A* 2016; **4**, 7903-13.

[14] M Cai, Y Wu, H Chen, X Yang, Y Qiang and L Han. Cost-performance analysis of perovskite solar modules. *Adv. Sci*. 2017; **4**, 1600269.

[15] K Rakstys, S Paek, P Gao, P Gratia, T Marszalek, G Grancini, KT Cho, K Genevicius, V Jankauskas, W Pisula and MK Nazeeruddin. Molecular engineering of face-on oriented dopant-free hole transporting material for perovskite solar cells with 19 % PCE. *J. Mater. Chem.* A 2017; **5**, 7811-5.

[16] MI Hossain, FH Alharbi and N Tabet. Copper oxide as inorganic hole transport material for lead halide perovskite based solar cells. *Sol. Energ.* 2015; **120**, 370-80.

[17] Z Liu, A Zhu, F Cai, L Tao, Y Zhou, Z Zhao, Q Chen, YB Cheng and H Zhou. Nickel oxide nanoparticles for efficient hole transport in p-i-n and n-i-p perovskite solar cells. *J. Mater. Chem. A* 2017; **5**, 6597-605.

[18] GM Arumugam, SK Karunakaran, C Liu, C Zhang, F Guo, S Wu and Y Mai. Inorganic hole transport layers in inverted perovskite solar cells: A review. *Nano Select* 2021; **2**, 1081-116.

[19] H Lei, G Yang, X Zheng, ZG Zhang, C Chen, J Ma, Y Guo, Z Chen, P Qin, Y Li and G Fang. Incorporation of high-mobility and room-temperature-deposited cuxs as a hole transport layer for efficient and stable organo-lead halide perovskite solar cells. *Solar RRL* 2017; **1**, 1700038.

[20] D Han, C Wu, Q Zhang, S Wei, X Qi, Y Zhao, Y Chen, Y Chen, L Xiao and Z Zhao. Solution-processed Cu9S5 as a hole transport layer for efficient and stable perovskite solar cells. *ACS Appl. Mater. Interfac.* 2018; **10**, 31535-40.

[21] W Ke, G Fang, H Lei, P Qin, H Tao, W Zeng, J Wang and X Zhao. An efficient and transparent copper sulfide nanosheet film counter electrode for bifacial quantum dot-sensitized solar cells. *J. Power Sourc.* 2014; **248**, 809-15.
[22] KJ Huang, JZ Zhang and Y Fan. One-step solvothermal synthesis of different morphologies CuS nanosheets compared as supercapacitor electrode materials. *J. Alloy. Comp.* 2015; **625**, 158-63.3
[23] H Rao, W Sun, S Ye, W Yan, Y Li, H Peng, Z Liu, Z Bian and C Huang. Solution-processed CuS NPs as an inorganic hole-selective contact material for inverted planar perovskite solar cells. *ACS Appl. Mater. Interfac.* 2016; **8**, 7800-5.
[24] X Jiang, Y Xie, J Lu, W He, L Zhu and Y Qian. Preparation and phase transformation of nanocrystalline copper sulfides (Cu9S8, Cu7S4 and CuS) at low temperature. *J. Mater. Chem*. 2000; **10**, 2193-6.
[25] JM Ball, MM Lee, A Hey and HJ Snaith. Low-temperature processed meso-superstructured to thin-film perovskite solar cells. *Energ. Environ. Sci.* 2013; **6**, 1739-43.
[26] P Docampo, JM Ball, M Darwich, GE Eperon and HJ Snaith. Efficient organometal trihalide perovskite planar-heterojunction solar cells on flexible polymer substrates. *Nat. Comm.* 2013; **4**, 2761.
[27] JY Jeng, KC Chen, TY Chiang, PY Lin, TD Tsai, YC Chang, TF Guo, P Chen, TC Wen and YJ Hsu. Nickel oxide electrode interlayer in $CH_3NH_3PbI_3$ perovskite/PCBM planar-heterojunction hybrid solar cells. *Adv. Mater*. 2014; **26**, 4107-13.
[28] T Kryshtab, VS Khomchenko, JA Andraca-Adame, VE Rodionov, VB Khachatryan and YA Tzyrkunov. The influence of doping element on structural and luminescent characteristics of ZnS thin films. *Superlattice. Microst.* 2006; **40**, 651-6.
[29] V Dimitrova and J Tate. Synthesis and characterization of some ZnS-based thin film phosphors for electroluminescent device applications. *Thin Solid Films* 2000; **365**, 134-8.
[30] J Kwak, J Lim, M Park, S Lee, K Char and C Lee. High-power genuine ultraviolet light-emitting diodes based on colloidal nanocrystal quantum dots. *Nano Lett*. 2015; **15**, 3793-9.
[31] DA Tonpe, KP Gattu, VV Kutwade, ME Sonawane, MC Sharma, H Jang, SH Han and R Sharma. ZnS-PANI nanocomposite with enhanced electrochemical performances for lithium-ion batteries. *J. Mater. Sci. Mater. Electron.* 2022; **33**, 18452-63.
[32] DV Dake, ND Raskar, VA Mane, RB Sonpir, HA Khawal, U Deshpande, E Stathatos and BN Dole. Photocatalytic performance of graphene-based Cr-substituted β ZnS nanocomposites. *Appl. Phys. Mater. Sci. Process.* 2022; **128**, 276.
[33] J Liu, C Gao, L Luo, Q Ye, X He, L Ouyang, X Guo, D Zhuang, C Liao, J Mei and W Lau. Low-temperature, solution processed metal sulfide as an electron transport layer for efficient planar perovskite solar cells. *J. Mater. Chem. A* 2015; **3**, 11750-5.
[34] W Ke, CC Stoumpos, JL Logsdon, MR Wasielewski, Y Yan, G Fang and MG Kanatzidis. TiO_2-ZnS corascade electron transport layer fefficient formamidinium tin iodide perovskite solar cells. *J. Am. Chem. Soc*. 2016; **138**, 14998-5003.
[35] J Li, C Kuang, M Zhao, C Zhao, L Liu, F Lu, N Wang, C Huang, C Duan, H Jian, L Yao and T Jiu. Ternary CuZnS nanocrystals: Synthesis, characterization, and interfacial application in perovskite solar cells. *Inorg. Chem.* 2018; **57**, 8375-81.
[36] J Tirado, C Roldán-Carmona, FA Muñoz-Guerrero, G Bonilla-Arboleda, M Ralaiarisoa, G Grancini, VIE Queloz, N Koch, MK Nazeeruddin and F Jaramillo. Copper sulfide nanoparticles as hole-transporting material in a fully-inorganic blocking layers n-i-p perovskite solar cells: Application and working insights. *Appl. Surf. Sci.* 2019; **478**, 607-14.
[37] M Popa, A Zakhidov and I Tiginyanu. Perovskite solar cells with ZnS as electron transport layer. *Proc. Rom. Acad. Math. Phys. Tech. Sci. Inform. Sci.* 2018; **19**, 559-66.
[38] T Oku. *Crystal structures of $CH_3NH_3PbI_3$ and related perovskite compounds used for solar cells*. *In*: LA Kosyachenko (Ed.). Solar Cells. IntechOpen, London, 2015.
[39] S Shahriar, C Sana, J Galindo, D Kava, D Hodges, E Castro, R Cotta, D Buck and L Echegoyen. Characterization and analysis of structural and optical properties of perovskite thin films. *In*: Proceedings of the IEEE 42nd Photovoltaic Specialist Conference *(*PVSC*)*, New Orleans. 2015.
[40] MI Ahmed, Z Hussain, M Mujahid, A Khan, SS Javaid and A Habib. Low resistivity ZnO-GO electron transport layer based CH3NH3PbI3 solar cells. *AIP Adv*. 2016; **6**, 065303.
[41] S Thangaraj, C Paramasivan, R Balusamy, S Arumainathan and P Thanigainathan. Evanescent wave optical fiber ammonia sensor with methylamine hydroiodide. *IET Optoelectronics* 2020; **14**, 292-5.
[42] S Hosseini and M Adelifard. The impact of cesium and antimony alloying on the photovoltaic properties of silver bismuth iodide compounds. *Phys. Status Solidi* 2021; **218**, 2000774.

[43] LI Ikhioya, UK Chime, CF Okoro, C Iroegbu, M Maaza and FI Ezema. Influence of dopant concentration on the electronic band gap energy of Yb-$ZrSe_2$ thin films for photovoltaic application via electrochemical deposition technique. *Mater. Res. Exp*. 2020; **7**, 026420.
[44] MH Khalil, RY Mohammed and MA Ibrahem. The influence of CBD parameters on the energy gap of ZnS Narcissus-like nanostructured thin films. *Coatings* 2021; **11**, 1131.
[45] O Malekan, MMB Mohagheghi and M Adelifard. The study of the morphology and structural, optical, and J-V characterizations of ($CH_3NH_3PbI_3$) perovskite photovoltaic cells in ambient atmosphere. *Scientia Iranica* 2021; **28**, 1939-52.
[46] NP Huse, AS Dive, KP Gattu and R Sharma. An experimental and theoretical study on soft chemically grown CuS thin film for photosensor application. *Mater. Sci. Semicond. Process*. 2017; **67**, 62-8.
[47] VV Kutwade, KP Gattu, AS Dive, ME Sonawane, DA Tonpe and R Sharma. Enhanced photosensing by Mg-doped ZnO hexagonal rods via a feasible chemical route. *J. Mater. Sci. Mater. Electron.* 2021; **32**, 6475-86.
[48] X Liu, Z Wu, X Fu, L Tang, J Li, J Gong and X Xiao. Highly efficient wide-band-gap perovskite solar cells fabricated by sequential deposition method. *Nano Energ*. 2021; **86**, 106114.
[49] B Lei, V O Eze and T Mori. Effect of morphology control of light absorbing layer on $CH_3NH_3PbI_3$ perovskite solar cells. *J. Nanoscience Nanotechnology* 2016; **16**, 3176-82.
[50] DA Tonpe, KP Gattu, VV Kutwade, ME Sonawane, AS Dive and R Sharma. Development of organic/inorganic PANI/ZnO 1D nanostructured hybrid thin film solar cell by soft chemical route. *J. Mater. Sci. Mater. Electron.* 2019; **30**, 16056-64.